Effective Potential and Superfluidity of Microwave-Shielded Polar Molecules

Fulin Deng,[1,2] Xing-Yan Chen,[3,4] Xin-Yu Luo,[3,4] Wenxian Zhang,[1,5] Su Yi,[2,6,7,*] and Tao Shi[2,6,7,†]
[1]School of Physics and Technology, Wuhan University, Wuhan, Hubei 430072, China
[2]CAS Key Laboratory of Theoretical Physics, Institute of Theoretical Physics, Chinese Academy of Sciences, Beijing 100190, China
[3]Max-Planck-Institut für Quantenoptik, 85748 Garching, Germany
[4]Munich Center for Quantum Science and Technology, 80799 München, Germany
[5]Wuhan Institute of Quantum Technology, Wuhan, Hubei 430206, China
[6]CAS Center for Excellence in Topological Quantum Computation and School of Physical Sciences, University of Chinese Academy of Sciences, Beijing 100049, China
[7]Peng Huanwu Collaborative Center for Research and Education, Beihang University, Beijing 100191, China

(Received 8 November 2022; revised 8 March 2023; accepted 9 April 2023; published 3 May 2023)

We analytically show that the effective interaction potential between microwave-shielded polar molecules consists of an anisotropic van der Waals–like shielding core and a modified dipolar interaction. This effective potential is validated by comparing its scattering cross sections with those calculated using intermolecular potential involving all interaction channels. It is shown that a scattering resonance can be induced under microwave fields reachable in current experiments. With the effective potential, we further study the Bardeen-Cooper-Schrieffer pairing in the microwave-shielded NaK gas. We show that the superfluid critical temperature is drastically enhanced near the resonance. As the effective potential is suitable for exploring the many-body physics of molecular gases, our results pave the way for studies of the ultracold gases of microwave-shielded molecular gases.

DOI: 10.1103/PhysRevLett.130.183001

Introduction.—Ultracold gases of polar molecules [1,2] provide a unique platform for exploring quantum information [3], quantum computing [4,5], quantum simulation [6,7], quantum chemistry [8,9], and precision measurement [10–12]. For more than one decade, tremendous experimental efforts have been paid to create the high-phase-space-density molecular gases [13–22]. Recently, degenerate Fermi gases of molecules have become available in experiments via the association of double degenerate atomic Bose-Fermi mixtures [23–25] and subsequent evaporative cooling [26–30]. Particularly, the stable molecular gases via the microwave shielding [29–32] provide an ideal platform for investigating strongly correlated many-body systems with the long-range and anisotropic dipole-dipole interaction (DDI) [33,34].

The DDI between microwave-shielded molecules (MSMs) is attractive in the plane of the microwave field. It may lead to exotic p-wave superfluids [35–37]. Remarkably, the microwave-dressing scheme provides tuning knobs to shape the shielding potential and to change the symmetry of DDI, which gives rise to distinct shape scattering resonances [32,38]. Across these resonances, a novel crossover [39–42] from a molecular superfluidity to a Bose-Einstein condensation (BEC) of tetramers may emerge. Theoretically, the simple model composed of a bare DDI and a short-range hard wall [35,36,43–47] fails to describe the microwave-induced scattering resonances, and thus, is inappropriate to study the superfluidity of MSMs. Yet, a complete description of the intermolecular interaction involving multiple dressed rotational states [31,48] is cumbersome for studies of many-body physics in a single shielded dressed state. Therefore, a simple and accurate effective potential is an essential ingredient for exploring the many-body physics of molecular gases.

In this Letter, we analytically derive an effective potential for two MSMs, and apply it to study the Bardeen-Cooper-Schrieffer (BCS) superfluidity in the NaK gas. At large intermolecular distance the potential is a negated DDI, while at short range it is of the $1/r^6$ type and anisotropically repulsive. Since the size of the DDI induced shielding core is much larger than that of the interatomic potential, the short-range part of the effective potential has a big impact on the two- and many-body physics. We then study the scattering of two molecules and show that the effective potential leads to the correct scattering cross sections and resonances. Finally, using the accurate effective potential, we find that the critical temperature of the BCS superfluidity can be efficiently enhanced via tuning the Rabi-frequency of the microwave field toward the scattering resonance. Not only is the well-behaved effective potential suitable for exploring the many-body physics, but it also provides a reliable guidance for the polar molecule experiments.

Effective molecule-molecule interaction.—We consider a gas of the NaK molecules in the $^1\Sigma(v=0)$ state which exhibits a molecular-frame dipole moment $d = 2.72$ debye.

 © 2023 American Physical Society

Under ultracold temperature, only the rotational degree of freedom is relevant such that the Hamiltonian of a single molecule is $\hat{h}_{\rm rot} = B_{\rm rot}\mathbf{J}^2$, where $B_{\rm rot}/\hbar = 2\pi \times 2.822$ GHz is the rotational constant and $\mathbf{J}$ is the angular momentum operator. Since the rotation spectrum, $B_{\rm rot}J(J+1)$, is anharmonic, we focus on the two lowest rotational manifolds ($J = 0$ and 1) which are split by an energy $\hbar\omega_e = 2B_{\rm rot}$. Correspondingly, the Hilbert space for the internal states of a molecule is defined by four states: $|J, M_J\rangle = |0,0\rangle$, $|1,0\rangle$, and $|1,\pm1\rangle$. Furthermore, the electric dipole moment of a molecule is $d\hat{\mathbf{d}}$, with $\hat{\mathbf{d}}$ being the unit vector along the internuclear axis of the molecule. For microwave shielding, molecules are illuminated by a position-independent elliptically polarized microwave field, $\mathbf{E}_{\rm mw} = E_{\rm mw}e^{-i\omega_0 t}e^{ik_z z}(\hat{\mathbf{e}}_1\cos\xi + \hat{\mathbf{e}}_{-1}\sin\xi) + \text{c.c.}$, propagating along the z axis, where $E_{\rm mw}$ is the amplitude of the microwave, ω_0 is the frequency of the microwave, $\hat{\mathbf{e}}_{\pm1} = \mp(\hat{\mathbf{e}}_x \pm i\hat{\mathbf{e}}_y)/\sqrt{2}$, and ξ is the elliptic angle.

Within the internal-state Hilbert space, the coupling between the microwave and the molecular rotational states gives rise to the Hamiltonian $\hat{h}_{\rm mw} = (\hbar\Omega/)2e^{-i\omega_0 t}|\xi_+\rangle\times\langle 0,0| + \text{H.c.}$, where $\Omega = 2E_{\rm mw}d/(\sqrt{3}\hbar)$ is the Rabi frequency and $|\xi_+\rangle \equiv \cos\xi|1,1\rangle + \sin\xi|1,-1\rangle$. Then, in the interaction picture, the eigenstates of the internal-state Hamiltonian, $\hat{h}_{\rm in} = \hat{h}_{\rm rot} + \hat{h}_{\rm mw}$, are $|0\rangle \equiv |1,0\rangle$, $|\xi_-\rangle \equiv \cos\xi|1,-1\rangle - \sin\xi|1,1\rangle$, $|+\rangle \equiv u|0,0\rangle + v|\xi_+\rangle$, and $|-\rangle \equiv u|\xi_+\rangle - v|0,0\rangle$, where $u = \sqrt{(1-\delta/\Omega_{\rm eff})/2}$ and $v = \sqrt{(1+\delta/\Omega_{\rm eff})/2}$ with $\delta = \omega_e - \omega_0$ being the detuning and $\Omega_{\rm eff} = \sqrt{\delta^2+\Omega^2}$ the effective Rabi frequency. The corresponding eigenenergies are $E_0 = E_{\xi_-} = \delta$ and $E_\pm = (\delta \pm \Omega_{\rm eff})/2$. Figure 1(a) schematically shows the level structure of a molecule.

For two molecules with dipole moments $d\hat{\mathbf{d}}_1$ and $d\hat{\mathbf{d}}_2$, the DDI between them is

$$V(\mathbf{r}) = \frac{d^2}{4\pi\epsilon_0 r^3}[\hat{\mathbf{d}}_1\cdot\hat{\mathbf{d}}_2 - 3(\hat{\mathbf{d}}_1\cdot\hat{\mathbf{r}})(\hat{\mathbf{d}}_2\cdot\hat{\mathbf{r}})], \qquad (1)$$

where ϵ_0 is the electric permittivity of vacuum, $r = |\mathbf{r}|$, and $\hat{\mathbf{r}} = \mathbf{r}/r$. To express DDI in the two-molecule internal Hilbert space, we note that the two-particle Hamiltonian $\hat{H}_2 = \sum_{j=1,2}\hat{h}_j + V(\mathbf{r}_1 - \mathbf{r}_2)$ possesses a parity symmetry, where $\hat{h}_j = -\hbar^2\nabla_j^2/(2M) + \hat{h}_{\rm in}(j)$ with M being the mass of the molecule. This suggests that the symmetric and antisymmetric two-particle internal states are decoupled in the Hamiltonian $\hat{H}_2$. Here, we focus on the ten-dimensional symmetric subspace in which the shielding states of the molecules lie. It turns out that, under the rotating-wave approximation, $V(\mathbf{r})$ in the seven-dimensional (7D) symmetric subspace, $\mathcal{S}_7 \equiv \{|\nu\rangle\}_{\nu=1}^7$, is decoupled from the remaining three-dimensional symmetric subspace, where $|1\rangle = |+,+\rangle$, $|2\rangle = |+,0\rangle_s$, $|3\rangle = |+,\xi_-\rangle_s$, $|4\rangle = |+,-\rangle_s$, $|5\rangle = |-,0\rangle_s$, $|6\rangle = |-,\xi_-\rangle_s$, and $|7\rangle = |-,-\rangle$ with $|i,j\rangle_s = (|i,j\rangle + |j,i\rangle)/\sqrt{2}$. Correspondingly, with respect to the asymptotical state $|\nu = 1\rangle$, the energies of these states are $\mathcal{E}_\nu = \{0, \frac{1}{2}(\delta - \Omega_{\rm eff}), \frac{1}{2}(\delta - \Omega_{\rm eff}), -\Omega_{\rm eff}, \frac{1}{2}(\delta - 3\Omega_{\rm eff}), \frac{1}{2}(\delta - 3\Omega_{\rm eff}), -2\Omega_{\rm eff}\}$. Below, we shall consider the two-molecule problem only in the subspace $\mathcal{S}_7$.

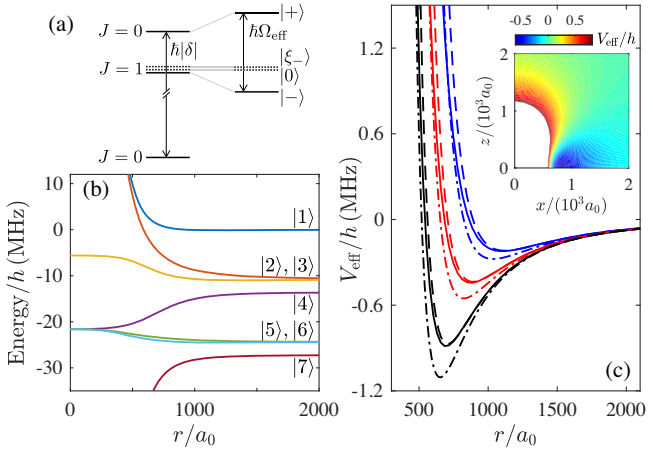

FIG. 1. (a) Schematic of the level structure of a microwave-dressed molecule. (b) Typical adiabatic potential curves of two colliding molecules for seven dressed state channels. (c) Effective potentials along $\theta = \pi/2$ obtained by numerical diagonalization (solid lines), numerical fitting (dashed line), and analytical expressions (dash-dotted lines) for $\xi = 0$, $\delta_r = 0.1$, and $\Omega/(2\pi) = 20$, 40, and 80 MHz (for three sets of curves in descending order). The inset maps out $V_{\rm eff}(\mathbf{r})/h$ (in units of MHz) on the xz plane for $\xi = 0, \delta_r = 0.1$, and $\Omega/(2\pi) = 50$ MHz, on which the white region corresponds to the shielding core.

To derive an effective potential between two molecules, we make use of the Born-Oppenheimer approximation which holds when the kinetic energy of the molecules is much smaller than the energy level spacings between internal states ($\sim\Omega_{\rm eff}$). After diagonalizing $V(\mathbf{r})$ in $\mathcal{S}_7$, we find seven adiabatic potentials corresponding to different dressed-state channels [see, e.g., Fig. 1(b) for the typical adiabatic potential curves]. Particularly, the effective potential for two molecules in the dressed state $|+\rangle$ is the highest adiabatic curve. Remarkably, as shown in Supplemental Material (SM), for small $\xi(\lesssim 15°)$ and $r^3 > d_0^2/(4\pi\epsilon_0\Omega)$, the effective potential for the highest channel is approximately

$$V_{\rm eff}(\mathbf{r}) = \frac{C_6}{r^6}\sin^2\theta\{1 - \mathcal{F}_\xi^2(\varphi) + [1-\mathcal{F}_\xi(\varphi)]^2\cos^2\theta\} + \frac{C_3}{r^3}[3\cos^2\theta - 1 + 3\mathcal{F}_\xi(\varphi)\sin^2\theta], \qquad (2)$$

where θ and φ are, respectively, the polar and azimuthal angles of $\mathbf{r}$ and $\mathcal{F}_\xi(\varphi) = \sin 2\xi\cos 2\varphi$. Moreover, $C_3 = d^2/[48\pi\epsilon_0(1+\delta_r^2)]$ and $C_6 = d^4/[128\pi^2\epsilon_0^2\Omega(1+\delta_r^2)^{3/2}]$ with $\delta_r = |\delta|/\Omega$. The C_3 term represents the modified DDI that is repulsive along the z axis and attractive in the

xy plane. In particular, for a circularly polarized microwave ($\xi = 0$), the C_3 term represents the negated DDI. When $\theta \neq 0$ or π, the C_6 term is repulsive since $|\mathcal{F}_\xi(\varphi)| \leq 1$ and thus provides a shielding core [49]. Interestingly, even along the z axis where the C_6 term vanishes, DDI itself is repulsive, which prevents two molecules from getting close to each other.

In Fig. 1(c), the effective potential Eq. (2) with $\xi = 0$ is benchmarked using the highest adiabatic curve obtained by numerically diagonalizing $V(\mathbf{r})$. Generally speaking, the expression for C_3 is accurate in the sense that it gives rise to the correct long-range behavior, while the analytical expression for C_6 is a good approximation only when $r^3 > d_0^2/(4\pi\epsilon_0\Omega)$. In any case, one can alternatively determine the values of C_3 and C_6 by fitting the adiabatic potential curve, which, as shown in Fig. 1(c), yields satisfactory results in the energy range of interest to us. We point out that further comparisons for the $\theta \neq 0$ and also $\xi \neq 0$ cases are presented in SM [50]. For an overall picture of the effective potential, we map out $V_{\text{eff}}(x, 0, z)$ in the inset of Fig. 1(c). In particular, the size of the shielding core roughly ranges from $600a_0$ to over $1000a_0$ which is significantly larger than that of the interatomic potentials.

Two-body scatterings.—To further justify the effective potential, we investigate the low-energy scattering of two molecules interacting via $V_{\text{eff}}(\mathbf{r})$. Since this study only involves a single scattering channel ($\nu = 1$ in $\mathcal{S}_7$), its results should be checked by the scattering calculations involving all seven channels. To this end, let us briefly outline the theoretical treatment for the multichannel scattering [31,32,48,51]. The Schrödinger equations governing the relative motion of two colliding molecules are

$$\sum_{\nu'=1}^{7}\left(-\frac{\hbar^2\nabla^2}{M}\delta_{\nu\nu'} + V_{\nu\nu'}\right)\psi_{\nu'}(\mathbf{r}) = \frac{\hbar^2 k_\nu^2}{M}\psi_\nu(\mathbf{r}), \quad (3)$$

where $\psi_\nu(\mathbf{r})$ is the wave function of the νth scattering channel, $V_{\nu\nu'} = \langle\nu|V|\nu'\rangle$, and $k_\nu = \sqrt{k_1^2 - M\mathcal{E}_\nu/\hbar^2}$ is the incident momentum of the νth scattering channel. To solve Eq. (3), we first expand the wave functions $\psi_\nu(\mathbf{r}) = \sum_{lm} Y_{lm}(\hat{\mathbf{r}})\phi_{\nu lm}(r)/r$ in the partial-wave basis, where l is odd for identical fermions. The equations for $\phi_{\nu lm}$ can be numerically evolved from $r = 0$ to a sufficiently large value r_∞ using Johnson's log-derivative propagator method [52]. Then, by comparing $\phi_{\nu lm}$ with the asymptotical boundary condition, we obtain the scattering amplitude $f_{\nu lm}^{\nu' l' m'}$ and cross section $\sigma_{\nu lm}^{\nu' l' m'} = 4\pi|f_{\nu lm}^{\nu' l' m'}|^2$ for the (νlm) to $(\nu' l' m')$ scattering. Numerically, to ensure the convergence of the scattering cross sections, we choose $k_0 r_\infty > 32$ and $l_c > 11$, where l_c is the truncation imposed on the orbital angular momentum. As a special case of the multichannel scattering, the Schrödinger equation for single-channel scattering can be obtained by projecting Eq. (3) in the

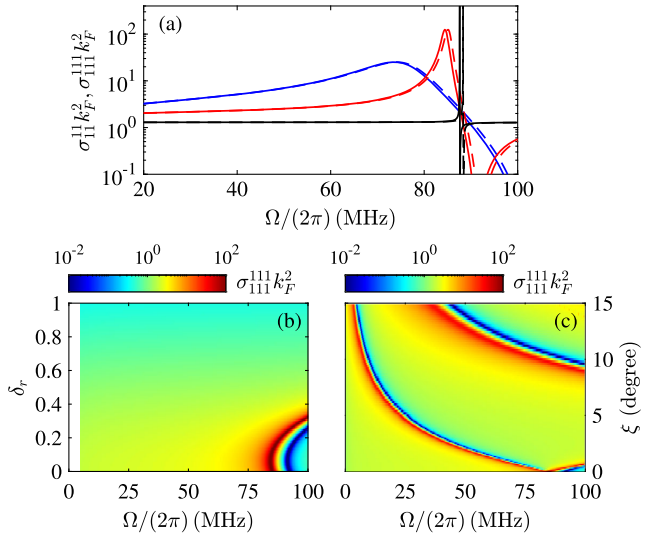

FIG. 2. (a) p-wave scattering cross sections $\sigma_{11}^{11}k_F^2$ (solid lines) and $\sigma_{111}^{111}k_F^2$ (dashed lines) as functions of Ω for $\xi = 0$, $\delta_r = 0.1$, and $k_1/k_F = 0.04$ (black lines), 0.45 (red lines), and 1 (blue lines). (b) and (c) are the distributions of $\sigma_{111}^{111}k_F^2$ on the Ω-δ_r plane with $\xi = 0$ and Ω-ξ plane with $\delta_r = 0.1$, respectively, for $k_1/k_F = 0.45$.

$\nu = 1$ channel with V_{11} being replaced by V_{eff}, and we denote the single-channel scattering cross section as $\sigma_{lm}^{l'm'}$.

For simplicity, we consider the $\xi = 0$ case for which the interaction possesses an axial symmetry. Here, we focus on the scattering cross section of the p wave since it is dominant over all other partial waves [50]. Figure 2(a) plots the Ω dependence of σ_{11}^{11} and σ_{111}^{111} for $\delta_r = 0.1$ and $k_1/k_F = 0.04$, 0.45, and 1, where $k_F = (6\pi^2 n_0)^{1/3}$ is the Fermi wave vector with $n_0 = 10^{12}$ cm^{-3} being the peak density of the experimentally realized molecular gas [30]. It is immediately noticed that, away from scattering resonances, quantitative agreements have been achieved for the p-wave cross section under different incident momenta. Moreover, the single-channel calculations can even predict the position of scattering resonance with high accuracy. As shown in SM, similar agreements are attained for other partial waves and even for the $\xi \neq 0$ case [50]. These results then validate the usage of the effective potential.

As to the properties of the p-wave cross section, we find that, for $k_1/k_F = 0.04$, σ_{111}^{111} barely changes as Ω varies over a wide range. A narrow scattering resonance then appears at $\Omega/(2\pi) \approx 87.7$ MHz, signaling the formation of a tetramer bound state. For $k_1/k_F = 1$, the resonant peak shifts to $\Omega/(2\pi) \approx 73.6$ MHz with the width of the resonance being significantly broadened. To understand these changes, let us recall that (1) there is a centrifugal barrier for the p-wave potential; (2) a scattering resonance at finite k_1 implies the incident particle is in resonance with a quasibound state localized inside the barrier. Now, as k_1 increases, the energy of the quasibound state in resonance with the incident particle also increases and gets closer to the top of the

barrier. Consequently, the lifetime of the quasibound state is shortened due to the large decay rate, which leads to a broader resonance. Furthermore, as k_1 grows, the quasibound state on resonance with the incident energy becomes shallower, which can be achieved by increasing C_6 or reducing Ω. Therefore, the resonant peak shifts toward the lower Ω direction with the increase k_1. Interestingly, the fact that the p-wave scattering cross section can be efficiently tuned via Ω implies that the short-range potential (i.e., C_6) can strongly influence the scattering properties due to the large shielding core.

In Fig. 2(b), we further map out σ_{111}^{111} on the Ω-δ_r plane for $\xi = 0$ and $k_1 = 0.45k_F$. A resonant peak clearly appears when the parameters satisfy $\delta_r \lesssim 0.3$ and $\Omega/(2\pi) \gtrsim 80$ MHz. To understand the relation between the position of the resonance and the microwave, we compute the WKB phase $\varphi_p \propto [d^8\Omega^2/(1+\delta_r^2)^5]^{1/12}$. A resonance occurs when φ is roughly $(n+0.1)\pi$ with n being an integer, which implies that φ_p must be sufficiently large to induce a resonance. This explains why the shape resonance appears in the parameter regime with large Ω and small δ_r.

Finally, we explore the relation between the scattering cross section and the elliptic angle. Figure 2(c) shows the distribution of σ_{111}^{111} on the Ω-ξ plan for $\delta_r = 0.1$ and $k_1/k_F = 0.45$. It is remarkable that the Rabi frequency required for shape resonance is dramatically lowered for nonzero ξ. Particularly, given $\xi \gtrsim 10°$, two shape resonances are observed and the first resonance emerges even when $\Omega/(2\pi)$ is below 10 MHz, a value accessible in current experiments [38]. The underlying reason for this observation is analyzed in detail in SM. Here, we present a qualitative explanation. For $\xi = 0$, the effective potential $V(\mathbf{r})$ has the cylindrical symmetry, while the positive ξ makes $V(\mathbf{r})$ lower along the y direction.

Superfluid phase transitions.—We now turn to explore the BCS superfluid phase transition in a homogeneous gas of MSMs. In particular, we focus on the effect of circularly polarized microwave field ($\xi = 0$) to the superfluidity. Since the inelastic cross sections are much smaller than that of elastic ones (see SM for details), we may safely construct the many-body Hamiltonian

$$\hat{H} = \int d^3\mathbf{r}\hat{\psi}^\dagger(\mathbf{r})\left(-\frac{\hbar^2\nabla^2}{2M} - \mu\right)\hat{\psi}(\mathbf{r}) + \frac{1}{2}\int d\mathbf{r}d\mathbf{r}'\hat{\psi}^\dagger(\mathbf{r})\hat{\psi}^\dagger(\mathbf{r}')V_{\text{eff}}(\mathbf{r}-\mathbf{r}')\hat{\psi}(\mathbf{r}')\hat{\psi}(\mathbf{r}) \quad (4)$$

in the single dressed-state channel $|+\rangle$, where $\hat{\psi}(\mathbf{r})$ is the annihilation operator of molecules and μ is the chemical potential.

In the superfluid phase, the order parameter takes the form

$$\Delta(\mathbf{k}) = \int \frac{d\mathbf{p}}{(2\pi)^3}\tilde{V}_{\text{eff}}(\mathbf{k}-\mathbf{p})\langle c_{-\mathbf{p}}c_{\mathbf{p}}\rangle, \quad (5)$$

where $\hat{c}_{\mathbf{p}} = \int d\mathbf{r}\hat{\psi}(\mathbf{r})e^{-i\mathbf{p}\cdot\mathbf{r}}/(2\pi)^{3/2}$ and the Fourier transform $\tilde{V}_{\text{eff}}(\mathbf{k}-\mathbf{p}) = (4\pi)^2\sum_{ll',m} i^{l'-l}Y_{lm}(\hat{k})Y^*_{l'm}(\hat{p})\tilde{V}_{ll',m}(k,p)$ of $V_{\text{eff}}(\mathbf{r})$ can be expanded in the partial-wave basis [50]. The mean-field theory gives the pairing function $\psi_\Delta(\mathbf{p}) \equiv \langle \hat{c}_{-\mathbf{p}}\hat{c}_{\mathbf{p}}\rangle = -\Delta(\mathbf{p})\tanh(\beta E_{\mathbf{p}}/2)/(2E_{\mathbf{p}})$, where $\beta = 1/(k_BT)$ is the inverse temperature and $E_{\mathbf{p}} = \sqrt{\varepsilon_{\mathbf{p}}^2 + |\Delta(\mathbf{p})|^2}$ is the dispersion of the Bogoliubov quasiparticle with $\varepsilon_{\mathbf{p}} = p^2/(2M) - \mu$. We point out that, unlike an ill-defined potential that requires renormalizations [36,39,43], the effective potential V_{eff} is well defined due to its repulsive core. In fact, the two-body wave function $\sim e^{-B/r^3}$ ($B > 0$) drops rapidly inside the shielding core, which guarantees that the integral in Eq. (5) is convergent. Thus, Eq. (5) is solvable without any interaction renormalization.

Close to the critical temperature T_c, $|\Delta(\mathbf{p})| \approx 0$ and, subsequently, $E_{\mathbf{p}} \approx \varepsilon_{\mathbf{p}}$. We can linearize Eq. (5) as

$$\Delta_{lm}(k) = -\frac{2}{\pi}\sum_{l'} i^{l'-l}\int_0^\infty p^2dp\tilde{V}_{ll',m}(k,p) \times \frac{\tanh(\beta_c\varepsilon_{\mathbf{p}}/2)}{2\varepsilon_{\mathbf{p}}}\Delta_{l'm}(p), \quad (6)$$

where $\beta_c = (k_BT_c)^{-1}$ and $\Delta(\mathbf{k}) = \sum_{lm}Y_{lm}(\hat{k})\Delta_{lm}(k)$. Because of the axial symmetry of the system, Δ_{lm} for different m's are decoupled. In the BCS regime, the chemical potential is approximated by the Fermi energy, i.e., $\mu \approx \varepsilon_F = \hbar^2k_F^2/(2M)$. Thus, Eq. (6) is equivalent to an eigenvalue problem of the integral Kernel, where the appearance of the first negative eigenvalue determines T_c.

It is worthwhile to note that $\tilde{V}_{11,m}$ contains a superficial divergent term contributed by the $1/r^6$ shielding potential, which can be regularized as $\tilde{V}_{11,m} \sim kp/r_{\text{UV}}$ by a short-range cutoff r_{UV} [50]. Different from the potential requiring renormalizations, $V_{ll',m}$ leads to the convergent solution of Eq. (6) as $r_{\text{UV}} \to 0$. A two-body calculation in the momentum space reveals that without $\tilde{V}_{11,m}$ a false bound state inside the shielding core would appear, while $\tilde{V}_{11,m}$ completely removes the false bound state and keeps two molecules away from each other. This regularization scheme can also be applied to interaction potentials of the form $1/r^n$, e.g., the Lennard-Jones potentials.

It is numerically found that the highest T_c is reached in the most attractive channel $m = \pm 1$, thus, hereafter we take $m = 1$. In all results presented below, the cutoff $k_Fr_{\text{UV}} \leq 10^{-8}$ (much smaller than the shielding core) and the truncation $l_c = 9$ of l are sufficient to ensure the convergence of the solution. In Fig. 3(a), we map out T_c on the Ω-δ_r plane away from scattering resonances where $T_c/\varepsilon_F \approx 0.137$ [40] reaches the BEC transition temperature and the weak-interaction assumption is violated. As can be seen, T_c can be enhanced by either increasing Ω or decreasing δ_r, since φ_p indicates that by both manners the

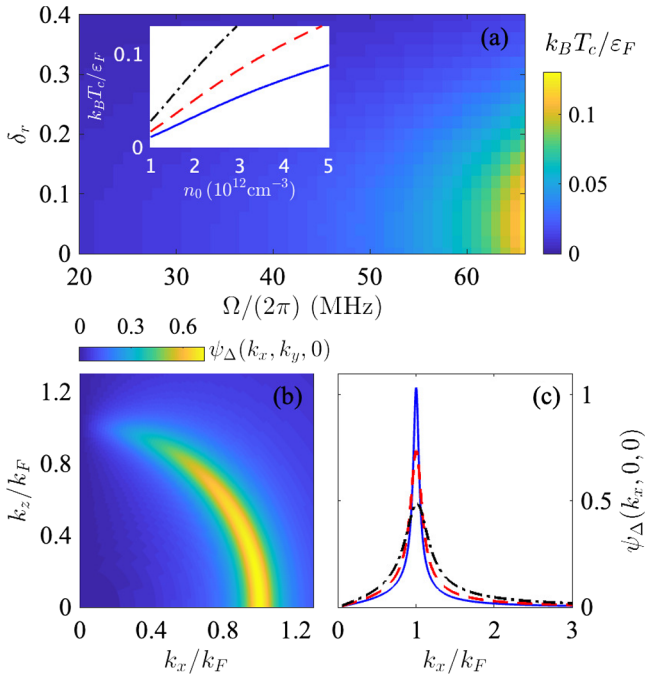

FIG. 3. (a) Critical temperature as a function of Ω and δ_r. The inset shows the n_0 dependence of T_c for $\delta_r = 0.1$ and $\Omega/(2\pi) = 28$ (solid line), 38 (dashed line), and 48 MHz (dash-dotted line). (b) Momentum distribution of the normalized pairing function $\psi_\Delta(k_x, 0, k_z)$ for $\delta = 0.1$ and $\Omega/(2\pi) = 58$ MHz. (c) The normalized pairing function $\psi_\Delta(k_x, 0, 0)$ along the k_x direction for $\delta_r = 0.1$ and $\Omega/(2\pi) = 48$ (solid line), 58 (dashed line), and 66 MHz (dash-dotted line). Unless otherwise stated, the density of the gas is $n_0 = 10^{12}$ cm^{-3} in this figure.

attractive interaction is enhanced. As Cooper pairs of molecules form around the Fermi surface, T_c is mainly determined by the scattering cross section at $k_1 \approx k_F$ which, as shown in Fig. 2(a), is very sensitive to the variation of Ω. Consequently, T_c can be efficiently tuned via the short-range potential C_6 even when the long-range dipolar interaction strength C_3 is fixed. The inset of Fig. 3(a) shows that T_c can also be increased as the density grows. In particular, for $\delta_r = 0.1$ and $\Omega/(2\pi) = 38$ MHz, T_c can be increased by roughly one order of magnitude as n_0 increases from 10^{12} to 5×10^{12} cm^{-3}.

In Fig. 3(b), the normalized $\psi_\Delta(\mathbf{k})$ on the k_x-k_z plane displays a clear anisotropic distribution peaked at the Fermi momentum k_F indicating the formation of Cooper pairs around the Fermi surface. The large occupation $\int k^2 dk |\int d\hat{\mathbf{k}} \psi_\Delta(\mathbf{k}) Y_{10}(\hat{\mathbf{k}})|^2 \gtrsim 0.97$ in the p wave channel implies that a p wave superfluidity [36,40,43,44,53] is achieved over a broad range of Rabi frequency due to the distinct scattering behavior of microwave shielded molecules. Finally, in Fig. 3(c) for $n_0 = 10^{12}$ cm^{-3} and $\delta_r = 0.1$, $\psi_\Delta(\mathbf{k})$ along the k_x direction shows the broadening peak width with increasing Ω, which indicates the formation of Cooper pairs over a broader momentum range under a stronger attractive interaction.

Conclusion and discussion.—In summary, we have derived an effective interaction potential for MSMs and validated it through two-body scattering calculations. We have also applied the effective potential to study the BCS superfluidity in the NaK gas and shown that the critical temperature can be greatly increased by tuning the Rabi frequency to a shape resonance. Since the typical size of the shielding core for MSMs is over several hundred Bohr radii, the short-ranged shielding potential cannot be naively replaced by a zero-range potential as that in atomic gases. This observation is of particular importance for fermionic molecules, as the molecules on Fermi surface is responsible for the BCS pairings. Therefore, the effective potential, particularly the short-range part, is essential for exploring the many-body physics of MSMs.

T. S. thanks Peng Zhang for the stimulating discussion. X.-Y. C. and X.-Y. L. thank the MPQ *NaK molecules* team for fruitful discussions. We thank Tijs Karman for stimulating discussions. This work was supported by National Key Research and Development Program of China (Grant No. 2021YFA0718304), by the NSFC (Grants No. 12135018, No. 11974363, No. 12047503, and No. 12274331), and by the Strategic Priority Research Program of CAS (Grant No. XDB28000000). X.-Y. C. and X.-Y. L. acknowledge support from the Max Planck Society, the European Union (PASQuanS Grant No. 817482) and the Deutsche Forschungsgemeinschaft under German Excellence Strategy—EXC-2111–390814868 and under Grant No. FOR 2247.

*syi@itp.ac.cn
†tshi@itp.ac.cn

[1] L. D. Carr, D. DeMille, R. V. Krems, and J. Ye, New J. Phys. **11**, 055049 (2009).
[2] S. Moses, J. Covey, M. Miecnikowski, D. Jin, and J. Ye, Nat. Phys. **13**, 13 (2017).
[3] P. Rabl, D. DeMille, J. M. Doyle, M. D. Lukin, R. J. Schoelkopf, and P. Zoller, Phys. Rev. Lett. **97**, 033003 (2006).
[4] D. DeMille, Phys. Rev. Lett. **88**, 067901 (2002).
[5] R. Sawant, J. A. Blackmore, P. D. Gregory, J. Mur-Petit, D. Jaksch, J. Aldegunde, J. M. Hutson, M. R. Tarbutt, and S. L. Cornish, New J. Phys. **22**, 013027 (2020).
[6] A. Micheli, G. K. Brennen, and P. Zoller, Nat. Phys. **2**, 341 (2006).
[7] E. Altman *et al.*, PRX Quantum **2**, 017003 (2021).
[8] R. V. Krems, Phys. Chem. Chem. Phys. **10**, 4079 (2008).
[9] M.-G. Hu, Y. Liu, D. D. Grimes, Y.-W. Lin, A. H. Gheorghe, R. Vexiau, N. Bouloufa-Maafa, O. Dulieu, T. Rosenband, and K.-K. Ni, Science **366**, 1111 (2019).
[10] V. V. Flambaum and M. G. Kozlov, Phys. Rev. Lett. **99**, 150801 (2007).
[11] T. A. Isaev, S. Hoekstra, and R. Berger, Phys. Rev. A **82**, 052521 (2010).
[12] J. J. Hudson, D. M. Kara, I. J. Smallman, B. E. Sauer, M. R. Tarbutt, and E. A. Hinds, Nature (London) **473**, 493 (2011).

[13] K.-K. Ni, S. Ospelkaus, M. H. G. de Miranda, A. Pe'er, B. Neyenhuis, J. J. Zirbel, S. Kotochigova, P. S. Julienne, D. S. Jin, and J. Ye, Science **322**, 231 (2008).
[14] T. Takekoshi, L. Reichsöllner, A. Schindewolf, J. M. Hutson, C. R. Le Sueur, O. Dulieu, F. Ferlaino, R. Grimm, and H.-C. Nägerl, Phys. Rev. Lett. **113**, 205301 (2014).
[15] J. W. Park, S. A. Will, and M. W. Zwierlein, Phys. Rev. Lett. **114**, 205302 (2015).
[16] F. Seeßelberg, N. Buchheim, Z.-K. Lu, T. Schneider, X.-Y. Luo, E. Tiemann, I. Bloch, and C. Gohle, Phys. Rev. A **97**, 013405 (2018).
[17] K. K. Voges, P. Gersema, M. Meyer zum Alten Borgloh, T. A. Schulze, T. Hartmann, A. Zenesini, and S. Ospelkaus, Phys. Rev. Lett. **125**, 083401 (2020).
[18] M. Guo, B. Zhu, B. Lu, X. Ye, F. Wang, R. Vexiau, N. Bouloufa-Maafa, G. Quéméner, O. Dulieu, and D. Wang, Phys. Rev. Lett. **116**, 205303 (2016).
[19] T. M. Rvachov, H. Son, A. T. Sommer, S. Ebadi, J. J. Park, M. W. Zwierlein, W. Ketterle, and A. O. Jamison, Phys. Rev. Lett. **119**, 143001 (2017).
[20] I. Stevenson, A. Z. Lam, N. Bigagli, C. Warner, W. Yuan, S. Zhang, and S. Will, Phys. Rev. Lett. **130**, 113002 (2022).
[21] W. B. Cairncross, J. T. Zhang, L. R. B. Picard, Y. Yu, K. Wang, and K.-K. Ni, Phys. Rev. Lett. **126**, 123402 (2021).
[22] N. Fitch and M. Tarbutt, *Advances In Atomic, Molecular, and Optical Physics* (Academic Press, 2021), pp. 157–262.
[23] L. D. Marco, G. Valtolina, K. Matsuda, W. G. Tobias, J. P. Covey, and J. Ye, Science **363**, 853 (2019).
[24] M. Duda, X.-Y. Chen, A. Schindewolf, R. Bause, J. von Milczewski, R. Schmidt, I. Bloch, and X.-Y. Luo, Nat. Phys. (2023).
[25] J. Cao, H. Yang, Z. Su, X.-Y. Wang, J. Rui, B. Zhao, and J.-W. Pan, Phys. Rev. A **107**, 013307 (2023).
[26] G. Valtolina, K. Matsuda, W. G. Tobias, J.-R. Li, L. De Marco, and J. Ye, Nature (London) **588**, 239 (2020).
[27] J.-R. Li, W. G. Tobias, K. Matsuda, C. Miller, G. Valtolina, L. De Marco, R. R. W. Wang, L. Lassablière, G. Quéméner, J. L. Bohn, and J. Ye, Nat. Phys. **17**, 1144 (2021).
[28] K. Matsuda, L. D. Marco, J.-R. Li, W. G. Tobias, G. Valtolina, G. Quéméner, and J. Ye, Science **370**, 1324 (2020).
[29] L. Anderegg, S. Burchesky, Y. Bao, S. S. Yu, T. Karman, E. Chae, K.-K. Ni, W. Ketterle, and J. M. Doyle, Science **373**, 779 (2021).
[30] A. Schindewolf, R. Bause, X.-Y. Chen, M. Duda, T. Karman, I. Bloch, and X.-Y. Luo, Nature (London) **607**, 677 (2022).
[31] T. Karman and J. M. Hutson, Phys. Rev. Lett. **121**, 163401 (2018).
[32] L. Lassablière and G. Quéméner, Phys. Rev. Lett. **121**, 163402 (2018).
[33] T. Lahaye, C. Menotti, L. Santos, M. Lewenstein, and T. Pfau, Rep. Prog. Phys. **72**, 126401 (2009).
[34] M. A. Baranov, M. Dalmonte, G. Pupillo, and P. Zoller, Chem. Rev. **112**, 5012 (2012).
[35] L. You and M. Marinescu, Phys. Rev. A **60**, 2324 (1999).
[36] M. A. Baranov, M. S. Mar'enko, V. S. Rychkov, and G. V. Shlyapnikov, Phys. Rev. A **66**, 013606 (2002).
[37] J. Levinsen, N. R. Cooper, and G. V. Shlyapnikov, Phys. Rev. A **84**, 013603 (2011).
[38] X.-Y. Chen, A. Schindewolf, S. Eppelt, R. Bause, M. Duda, S. Biswas, T. Karman, T. Hilker, I. Bloch, and X.-Y. Luo, Nature (London) **614**, 59 (2023).
[39] C. A. R. Sá de Melo, M. Randeria, and J. R. Engelbrecht, Phys. Rev. Lett. **71**, 3202 (1993).
[40] M. Iskin and C. A. R. Sá de Melo, Phys. Rev. Lett. **96**, 040402 (2006).
[41] T. Shi, S.-H. Zou, H. Hu, C.-P. Sun, and S. Yi, Phys. Rev. Lett. **110**, 045301 (2013).
[42] R. Qi, Z.-Y. Shi, and H. Zhai, Phys. Rev. Lett. **110**, 045302 (2013).
[43] M. A. Baranov, L. Dobrek, and M. Lewenstein, Phys. Rev. Lett. **92**, 250403 (2004).
[44] K. V. Samokhin and M. S. Mar'enko, Phys. Rev. Lett. **97**, 197003 (2006).
[45] T. Shi, J.-N. Zhang, C.-P. Sun, and S. Yi, Phys. Rev. A **82**, 033623 (2010).
[46] C. Wu and J. E. Hirsch, Phys. Rev. B **81**, 020508(R) (2010).
[47] C. Zhao, L. Jiang, X. Liu, W. M. Liu, X. Zou, and H. Pu, Phys. Rev. A **81**, 063642 (2010).
[48] T. Karman, Z. Z. Yan, and M. Zwierlein, Phys. Rev. A **105**, 013321 (2022).
[49] A. V. Gorshkov, P. Rabl, G. Pupillo, A. Micheli, P. Zoller, M. D. Lukin, and H. P. Büchler, Phys. Rev. Lett. **101**, 073201 (2008).
[50] See Supplemental Material at http://link.aps.org/supplemental/10.1103/PhysRevLett.130.183001 for a detailed derivation of the effective potential, the numerical procedure for the scattering calculation, and the effective potential in the momentum space.
[51] A. V. Avdeenkov and J. L. Bohn, Phys. Rev. Lett. **90**, 043006 (2003).
[52] B. Johnson, J. Comput. Phys. **13**, 445 (1973).
[53] J. P. Gaebler, J. T. Stewart, J. L. Bohn, and D. S. Jin, Phys. Rev. Lett. **98**, 200403 (2007).